Inorg. Chem. **2006**, *45*, 9381–9386

Structure and Thermoelectric Characterization of $Ba_8Al_{14}Si_{31}$

Cathie L. Condron,[†] J. Martin,[‡] G. S. Nolas,[‡] Paula M. B. Piccoli,[§] Arthur J. Schultz,[§] and Susan M. Kauzlarich*,[†]

Department of Chemistry, University of California, One Shields Avenue, Davis, California 95616, and Department of Physics, University of South Florida, Tampa, Florida 33620, and Intense Pulsed Neutron Source, Argonne National Laboratory, Argonne, Illinois 60439-4814

Received July 5, 2006

A molten Al flux method was used to grow single crystals of the type I clathrate compound $Ba_8Al_{14}Si_{31}$. Single-crystal neutron diffraction data for $Ba_8Al_{14}Si_{31}$ were collected at room temperature using the SCD instrument at the Intense Pulsed Neutron Source, Argonne National Laboratory. Single-crystal neutron diffraction of $Ba_8Al_{14}Si_{31}$ confirms that the Al partially occupies all of the framework sites (R1 = 0.0435, wR2 = 0.0687). Stoichiometry was determined by electron microprobe analysis, density measurements, and neutron diffraction analysis. Solid-state ^{27}Al NMR provides additional evidence for site preferences within the framework. This phase is best described as a framework-deficient solid solution $Ba_8Al_{14}Si_{31}$, with the general formula, $Ba_8Al_xSi_{42-3/4x}[]_{4-1/4x}$ ([] indicates lattice defects). DSC measurements and powder X-ray diffraction data indicate that this is a congruently melting phase at 1416 K. Temperature-dependent resistivity reveals metallic behavior. The negative Seebeck coefficient indicates transport processes dominated by electrons as carriers.

Introduction

A good thermoelectric material requires the combination of high electrical conductivity (σ) or low electrical resisitivity (ρ), low-thermal conductivity (κ), and high thermopower or Seebeck coefficient (S), ultimately resulting in a high figure of merit ($zT = S^2T/\rho\kappa$, where T is temperature).[1] Materials that best meet these requirements are typically heavily doped, small band-gap semiconductors or semimetals. Such materials provide a balance between the high Seebeck coefficient of semiconductors and the low electrical resistivity of metals.

Light element-containing materials have, in general, been ignored for thermoelectric applications because they fall outside of the accepted criteria for finding good thermoelectric materials. In general, materials that contain light elements lack the required heavy elements which contribute to lowering the lattice thermal conductivity by scattering phonons. However, Si−Ge alloys,[2] transition metal disilicides,[3−5] metal chalcogenides,[6,7] several boron compounds,[8,9] and the oxide material $TiO_{1.1}$,[10] have attracted attention for high-temperature thermoelectric applications. In particular, n-type SiGe has provided a high figure of merit and remains a unique light-element material for thermoelectric applications.[2,11] Additionally, ternary clathrate phases, which combine a small amount of heavy atoms within a light-atom framework, show excellent thermoelectric figures of merit,[12−14] as recently exemplified by $Ba_8Ga_{16}Ge_{30}$ grown using the Czochralski method showing a zT of 1.35 at 900 K.[15] Although the $A_8Ga_{16}Ge_{30}$ (A = alkaline earth or rare earth element) systems have been extensively studied for thermoelectric proper-

* To whom correspondence should be addressed. E-mail: smkauzlarich@ucdavis.edu. Phone: (530) 752-4756. Fax: (530) 752−8995.
[†] University of California Davis.
[‡] University of South Florida.
[§] Argonne National Laboratory.

(1) Wood, C. *Rep. Prog. Phys.* **1988**, *51*, 459.
(2) Bhandari, C. M.; Rowe, D. M. *Thermal Conduction in Semiconductors*; Wiley Eastern Limited: New Delhi, India, 1988.
(3) Nishida, I. *Phys. Rev. B* **1973**, *7*, 2710.
(4) Nishida, I.; Sakata, T. *J. Phys. Chem. Solids* **1978**, 499.
(5) Kojima, T. *Phys. Status Solidi A* **1989**, *111*, 233.
(6) Bass, J. C.; Elsner, N. B. In *3rd International Conference on Thermoelectric Energy Conversion*; Rao, K. R., Ed.; IEEE: Piscataway, NJ, 1980; p 8.
(7) Nakahara, J. F.; Takeshita, T.; Tschetter, M. J.; Beaudry, B. J.; Gschneidner, K. A., Jr. *J. Appl. Phys.* **1988**, *63*, 2331.
(8) Wood, C.; Emin, D. *Phys. Rev. B* **1984**, *29*, 4582.
(9) Yugo, S.; Sato, T.; Kimura, T. *Appl. Phys. Lett.* **1985**, *7*, 111.
(10) Okinaka, N.; Akiyama, T. In *2005 International Conference on Thermoelectrics*; IEEE: Piscataway, NJ, 2005; p 34.
(11) Slack, G. A.; Housain, M. A. *J. Appl. Phys.* **1991**, *70*, 2694.
(12) Cohn, J. L.; Nolas, G. S.; Fessatidis, V.; Metcalf, T. H.; Slack, G. A. *Phys. Rev. Lett.* **1999**, *82*, 779.
(13) Nolas, G. S. *Mater. Res. Soc. Symp. Proc.* **1999**, *545*, 435.
(14) Nolas, G. S.; Weakley, T. J. R.; Cohn, J. L.; Sharma, R. *Phys. Rev. B.* **2000**, *61*, 3845.
(15) Saramata, A.; Svensson, G.; Palmqvist, A. E. C.; Stiewe, C.; Mueller, E.; Platzek, D.; Williams, S. G. K.; Rowe, D. M.; Bryan, J. D.; Stucky, G. D. *J. Appl. Phys.* **2006**, *99*, 023708.

10.1021/ic061241w CCC: $33.50
Published on Web 10/18/2006

ties,[12,16−20] the Al−Si phases have only been studied superficially,[21,22] and there have been no reports on property optimization.

Along with glasslike thermal conductivity, high electrical conductivity, high Seebeck coefficient, and stability in air, acids, and bases, clathrate phases have the added advantage of using light elements to form potential thermoelectric materials. In addition, clathrate phases can use different combinations of elements in both the cages and framework, allowing for fine-tuning of the properties with subtle changes in composition.

We have previously presented the synthesis, structure, Raman spectroscopy, and magnetism of Ba/Eu Al−Si containing clathrate phases.[23] This paper presents single-crystal neutron diffraction data for $Ba_8Al_{14}Si_{31}$, and the defect model of the clathrate structure is reevaluated. Electron microprobe analysis and density measurements provide stoichiometry. TGA/DSC data indicate that this is a congruently melting phase 1416 K. The resistivity, Seebeck coefficient, and thermal conductivity as a function of temperature for $Ba_8Al_{14}Si_{31}$ are also provided.

Experimental Section

Synthesis. Details of the synthetic procedures, along with electron microprobe data and density measurements for $Ba_8Al_{14}Si_{31}$, have been reported previously.[23] Briefly, electron microprobe analysis was performed with a Cameca SX-100 electron microprobe equipped with five wavelength-dispersive spectrometers, operating at 10 nA of current with a 20 keV accelerating potential. Several crystals obtained from different reactions were mounted in epoxy and polished for analysis. Totals from all analyses were 100%, and the compositions were homogeneous within the crystals. Elemental compositions were within standard deviation or identical between crystals. The stoichiometry was previously reported to be (Ba/Al/Si) 7.5(2):13.0(1):29.2(2).[23] However, if Ba is assumed to be 8.0, then the relative stoichiometry of Ba/Al/Si is 8.0(2):14.0(1):31.1(2).

Density Measurements. The density of $Ba_8Al_{14}Si_{31}$ was measured using the flotation method. In the flotation method, the crystal is suspended in a mixture of liquids, one lighter and one heavier than the crystal of which the proportions are adjusted until the crystal remains suspended in the medium. The density of the liquid, determined by weighing a sample of known volume, is the density of the crystal.[24] The liquids used were CH_2I_2 ($D = 3.31$) and CH_2Cl_2 ($D = 1.316$).

Table 1. Crystal Data and Structure Refinement for $Ba_8Al_{14}Si_{31}$

temp (K)	298
radiation	neutron
data collection technique	time-of-flight Laue
space group	$Pm\bar{3}n$ (No. 223)
lattice params (Å)	10.625(10)
vol (Å^3)	1199.5(2)
Z	1
density (calcd) (Mg/m^3)	3.25
abs coeff (cm^{-1})	0.015
reflns collected	1759
independent Reflns	234
data/restraints/params	234/0/17
GOF on F^2	1.019
final R indices [$I > 2\sigma(I)$][a]	R1 = 0.0435
	wR2 = 0.0687
R indices (all data)	R1 = 0.0520
	wR2 = 0.0698
extinction coeff	1.265×10^{-4}(6)
largest diff. peak and hole (fm Å^{-3})	0.275 and −0.296

[a] $R1 = [\sum||F_0| - |F_c||]/\sum|F_0|$; $wR2 = \{[\sum w[(F_0)^2 - (F_c)^2]^2]\}^{1/2}$; $w^{-1} = [\sigma^2(F_0) + (0.0471P)^2 + (0.5945P)]$, where $P = [\max(F_o^2,0) + 2F_c^2/3]$

Table 2. Atomic Coordinates and Equivalent Isotropic Displacement Parameters (U_{eq})[a] for $Ba_8Al_{14}Si_{31}$

atom	site	x	y	z	U_{eq} (Å^2)	occupancy
Ba(1)	2a	0	0	0	0.0140(8)	1
Ba(2)	6d	0	0.25	0.5	0.0324(7)	1
M(1)	6c	0.25	0	0.5	0.0135(7)	0.965[b]
M(2)	16i	0.18513(9)	0.18513	0.18513	0.0131(4)	0.965[b]
M(3)	24k	0.11776(14)	0	0.30551(12)	0.0118(3)	0.965[b]

[a] U_{eq} is defined as one-third of the trace of the orthogonalized U^{ij} tensor. [b] Determined from electron microprobe analysis.

Single-Crystal Neutron Diffraction. Single-crystal neutron diffraction data for $Ba_8Al_{14}Si_{31}$ were collected using the SCD instrument at the Intense Pulsed Neutron Source, Argonne National Laboratory.[25−27] The room-temperature measurements were carried out on a single crystal of $Ba_8Al_{14}Si_{31}$ with approximate dimensions of $3 \times 1 \times 0.85$ mm^3 and a weight of 8 mg, which was glued to an aluminum pin. The SCD beam line employs a white beam time-of-flight Laue technique with a diffractometer equipped with two position-sensitive area detectors. Details of the data collection and analysis procedures have been published previously.[28] The GSAS software package was used for structural analysis.[29] The atomic positions of the X-ray diffraction structure were used as a starting point in the refinement. The refinement was based on F^2 with a minimum d spacing of 0.8 Å. In the final refinement, all atoms were refined with anisotropic displacement parameters. Data collection and refinement parameters are summarized in Tables 1−3.

NMR. A Bruker AVANCE500 MHz spectrometer equipped with a fast digitizer was used with a Bruker high-speed MAS probe. The sample was placed in a 2.5 mm zirconia rotor. A one-pulse experiment was carried out with the sample spinning at 28.26 kHz. A 2 μs pulse was used at a resonance frequency of 130.316 MHz. The 90° pulse was found to be 4 μs, and a total of 5816 scans were collected with a 0.5 μs dwell time and a 0.2 s relaxation delay. The Bruker XWINNMR3.5 software was used to record and process the data.

(16) Blake, N. P.; Latturner, S.; Bryan, J. D.; Stucky, G. D.; Metiu, H. *J. Chem. Phys.* **2001**, *115*, 8060.
(17) Blake, N. P.; Mollnitz, L.; Kresse, G.; Metiu, H. *J. Chem. Phys.* **1999**, *111*, 3133.
(18) Chakoumakos, B. C.; Sales, B. C.; Mandrus, D. G.; Nolas, G. S. *J. Alloys Compd.* **2000**, *296*, 80.
(19) Keppens, V.; McGuire, M. A.; Teklu, A.; Laermans, C.; Sales, B. C.; Mandrus, D.; Chakoumakos, B. C. *Phys. B* **2002**, *316*−*317*, 95.
(20) Nolas, G. S.; Cohn, J. L.; Slack, G. A.; Schujman, S. B. *Appl. Phys. Lett.* **1998**, *73*, 178.
(21) Mudryk, Y.; Rogl, P.; Paul, C.; Berger, S.; Bauer, E.; Hilscher, G.; Godart, C.; Noel, H.; Saccone, A.; Ferro, R. *Phys. B* **2003**, *328*, 44.
(22) Mudryk, Y.; Rogl, P.; Paul, C.; Berger, S.; Bauer, E.; Hilscher, G.; Godart, C.; Noel, H. *J. Phys.: Condens. Matter* **2002**, *14*, 7991.
(23) Condron, C. L.; Porter, R.; Guo, T.; Kauzlarich, S. M. *Inorg. Chem.* **2005**, *44*, 9185.
(24) Stout, G. H.; Jensen, L. H. In *X-ray Structure Determination: A Practical Guide*, 2nd ed.; John Wiley and Sons Inc.: New York, 1989; p 89.
(25) Schultz, A. J.; Teller, R. G.; Williams, J. M.; Lukehart, C. M. *J. Am. Chem. Soc.* **1984**, *106*, 999.
(26) Schultz, A. J.; Van Derveer, D. G.; Parker, D. W.; Baldwin, J. E. *Acta Crystallogr. C* **1990**, *46*, 276.
(27) Schultz, A. J. *Trans. Am. Crystallogr. Assoc.* **1987**, *23*, 61.
(28) Jacobson, R. A. *J. Appl. Phys.* **1976**, *19*, 283.
(29) Larson, A. C.; Von Dreele, R. B. Los Alamos National Laboratory, Los Alamos, NM, 2000.

Table 3. Refined Occupancies for Si and Calculated Al/Si Occupancies Assuming a Total Occupancy of 0.965 for Each Framework Site

atom	site	refined Si occupancy	f^a	Al occupancy^b	Si occupancy^b	total Al	total Si
M1	6c	0.876(13)	0.363	0.547	0.438	3.28	2.62
M2	16i	0.921(9)	0.382	0.270	0.704	4.32	11.26
M3	24k	0.921(9)	0.382	0.270	0.704	6.48	16.89
All		0.915(8)	0.380	0.306	0.669	14.08	30.77

[a] Product of the refined Si occupancy times the Si scattering length (b_{Si} = 0.41491). [b] Obtained from $f = 0.965[xb_{Al} + (1 - x)b_{Si}]$, where $0.965x$ is the Al occupancy and $0.965(1 - x)$ is the Si occupancy.

TGA/DSC. A Netzsch Thermal Analysis STA 409 STA was used to evaluate the thermal properties of $Ba_8Al_{14}Si_{31}$ between 298 and 1500 K. After a baseline was established, several crystals were ground into a powder (40−60 mg) and placed into alumina crucibles which were heated under argon at 10 K/min with an acquisition rate of 4 pts/K.

Thermoelectric Property Measurements. The crystal was cut with a wire saw, to minimize surface damage, in the shape of a parallelepiped for transport measurements. The thermoelectric properties were performed similarly to that reported previously with a few modifications.[30] Temperature-dependent four-probe electrical resistivity, steady-state Seebeck coefficient, and thermal conductivity measurements were simultaneously performed using a custom-designed closed-cycle refrigerator employing a differential thermocouple to measure the temperature gradient and 0.001 in. copper wires soldered to small nickel-plated dots in the specimen for the voltage measurements.

Four-probe Hall measurements were conducted at both positive and negative magnetic-field directions to eliminate effects resulting from voltage-probe misalignment.

Results and Discussion

The clathrate type I structure of the heavier group 13- and 14-containing phases has been well-studied, in particular, for their high potential as materials for thermoelectric applications. Clathrate compounds consist of covalently bonded framework atoms that encapsulate either electron-donating or electron-accepting guest atoms. In this example the framework is composed of Al and Si atoms, and the electron-donating guest is Ba. The clathrate type I structure contains three crystallographically distinct framework sites, which are listed in Table 2 and can be seen in Figure 1. Each site is tetrahedrally coordinated to four other framework atoms and is distorted from an ideal tetrahedral environment by different degrees. The degree of distortion in the local environments of each framework site, along with the relative stoichiometry of the various framework elements plays a key role in understanding and determining the structure and how it affects the properties. Previous studies suggest the 6c site is preferentially filled by groups 12 and 13, as well as transition metal framework elements.[31−33] This is indeed the case reported for $Ba_8Ga_{16}Si_{30}$,[34] where the majority of the gallium is located in the 6c and 24k sites.[34,35] Because the electron densities and thus the X-ray scattering power of Al and Si are very similar, it is difficult to distinguish between them during refinement of the X-ray data. Mudryk et al. assigned the Al to the 6c position on the basis of bond-length analysis for the stoichiometry $Eu_2Ba_6Al_8Si_{36}$. However, for $Ba_8Al_{14}Si_{31}$ and $Eu_{0.52}Ba_{7.5}Al_{16}Si_{30}$, which we previously investigated,[23] the framework bond lengths are not significantly different from one another, and therefore no distinction between Al and Si could be assumed.

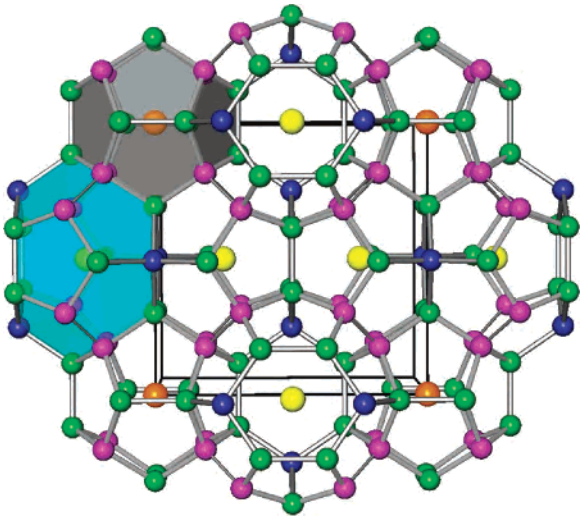

Figure 1. Polyhedral structure of the type 1 clathrate. Framework atoms are designated by color. The 6c sites are blue; the 16i sites are purple, and the 24k sites are green. The 2a sites are orange, and the 6d sites are yellow. The crystal structure was generated by Balls and Sticks.[42]

Several compositions of the $Ba_8Al_{16}Si_{30}$-type phase have been investigated and most are considered to be framework-deficient solid solutions with the general formula of $Ba_8Al_xSi_{42-3/4x}[]_{4-1/4x}$ (x = 8, 12, 16; [] indicates lattice defects). The phases, $Ba_8Al_{16}Si_{30}$ and $Ba_8Al_{10}Si_{33}$ have been reported to melt incongruently. We have reported the structure and composition of a framework-deficient phase, $Ba_{7.5}Al_{13}Si_{29}$.[23]

To further investigate the site preference of Al in the ternary Al/Si framework clathrates, single-crystal neutron diffraction studies were performed on $Ba_8Al_{14}Si_{31}$. Details of the neutron data collection and structure refinement are provided in Table 1, and atomic coordinates and equivalent isotropic displacement parameters are provided in Table 2. Neutron diffraction data are more sensitive to Al/Si occupancies than X-ray data because the relative difference in scattering lengths (b_{Al} = 0.3449 × 10^{-12} cm and b_{Si} = 0.41491 × 10^{-12} cm) is greater than the relative difference in the number of electrons (13 vs 14). Furthermore, neutron-scattering lengths are constant for all angles and wavelengths, and thus there is no correlation of the form factor with the thermal parameters as is the case with X-ray diffraction.

The neutron data were initially refined with the occupancies fixed and the Si/Al ratio allowed to vary. This refinement

(30) Martin, J.; Erickson, S.; Nolas, G. S.; Alboni, P.; Tritt, T. M.; Yang, J. *J. Appl. Phys.* **2006**, *99*, 044903.
(31) Bentien, A.; Christensen, M.; Bryan, J. D.; Sanchez, A.; Paschen, S.; Steglich, F.; Stucky, G. D.; Iversen, B. B. *Phys. Rev. B.* **2004**, *69*, 045107/045101.
(32) Kuhl, B.; Czybulka, A.; Schuster, H.-U. *Z. Anorg. Allg. Chem.* **1995**, *621*, 1.
(33) Cordier, G.; Woll, P. *J. Less-Common Met.* **1991**, *169*, 291.
(34) Eisenmann, B.; Schaefer, H.; Zagler, R. *J. Less-Common Met.* **1986**, *118*, 43.
(35) Latturner, S. E.; Bryan, J. D.; Blake, N.; Metiu, H.; Stucky, G. D. *Inorg. Chem.* **2002**, *41*, 3956.

yielded an approximately 50:50 Si/Al ratio on both the 16i and 24k sites, and the 6c site refined to give 4Al and 2Si, giving a stoichiometry of $Ba_8Al_{23.39}Si_{21.61}$. This stoichiometry is not correct according to the elemental ratios obtained from electron microprobe analysis. Additionally, the scattering amplitude from each site is the product of the occupancy and the scattering length, such that only one of which can be varied. It is well-known that these clathrate phases can have both variable stoichiometry and defects on the framework sites. Taking this into account, we performed the final refinements with the Ba sites fully occupied and with a scattering amplitude that corresponds to the total Al/Si ratio given by electron microprobe analysis, which provides a framework-deficient model with framework site occupancy of 0.965. Thus, Si only was put into the framework positions, and the Si occupancies were allowed to refine. The refined Si occupancies are given in Table 3. The scattering amplitude, f, on each site is the product of the refined Si occupancy and the Si neutron scattering length, b_{Si}. With the necessary (otherwise, there are too many variables) but not entirely correct assumption that all three crystallographic sites have a total Al + Si occupancy of 0.965, the individual Al and Si occupancies were calculated using the equation $f = 0.965-[xb_{Al} + (1 - x)b_{Si}]$, where $0.965x$ is the Al occupancy and $0.965(1 - x)$ is the Si occupancy. Refinement parameters and results using this model are given in Table 3. These results clearly indicate that site M1 (6c) has higher relative Al occupancy than sites M2 and M3, which is in complete agreement with the NMR analyses (vide infra). Furthermore, the overall occupancies agree with a nominal stoichiometry of $Ba_8Al_{14}Si_{31}$, which is in close agreement with the electron microprobe analysis and the density measurement. These results allow us to say with confidence that Al is present on every site. Additionally, since the 6c site has more Al than Si, we can say that Al preferentially fills the 6c site, which is consistent with previous suggestions that group 12 and 13 elements preferentially fill the 6c site before filling the 16i and 24k sites.[31−33,35]

These results indicate that the cation vacancy model previously proposed[23] is not correct. If the Ba sites are considered to be fully occupied, the composition of the phase, $Ba_{7.5}Al_{13}Si_{29}$, which we previously reported,[23] is better reported as $Ba_8Al_{13.95}Si_{31.12}$ or $Ba_8Al_{16-x}Si_{30+x}$, where $x = 1.06$, which is consistent with the elemental ratios provided by electron microprobe analysis. This is also consistent with the general formula $Ba_8Al_xSi_{42-3/4x}[]_{4-1/4x}$ that has been proposed by Mudryk et al. for $Ba_8Al_{16}Si_{30}$.[21] The general formula $Ba_8Al_xSi_{42-3/4x}[]_{4-1/4x}$ assumes Zintl-like behavior implying that these phases should display semiconducting behavior. However, $Ba_8Al_{14}Si_{31}$ and the Al−Si framework clathrates reported by Mudryk et al. are metallic. Therefore, although the general formula given above expresses the solid solution well, slight deviations from ideal stoichiometry lead to metallic properties and, in this case, n-type conduction.

To provide additional support for this model, density measurements were revisited. In our previous report,[23] the densities were measured using the Archimedes method. However, there can be significant errors because of inclusions of Al in the crystals or with wetting the surface of the crystals. The densities were remeasured using the flotation method.[24] The measured densities, along with calculated densities for different elemental ratios, are given in Table 4. The data are consistent with the defect model described above, although experimental density measurements are typically lower than the actual density of the sample.

Table 4. Calculated and Measured Densities (mg/mL) for $Ba_8Al_{14}Si_{31}$[a]

stoichiometry	calcd	measured
$Ba_{7.5}Al_{13}Si_{29}$	3.04	
$Ba_8Al_{14}Si_{31}$	3.25	3.23
$Ba_8Al_{16}Si_{30}$	3.29	

[a] Measured densities were obtained using the flotation method with CH_2I_2 ($d = 3.31$ mg/ml) and CH_2Cl_2 ($d = 1.316$ mg/mL).

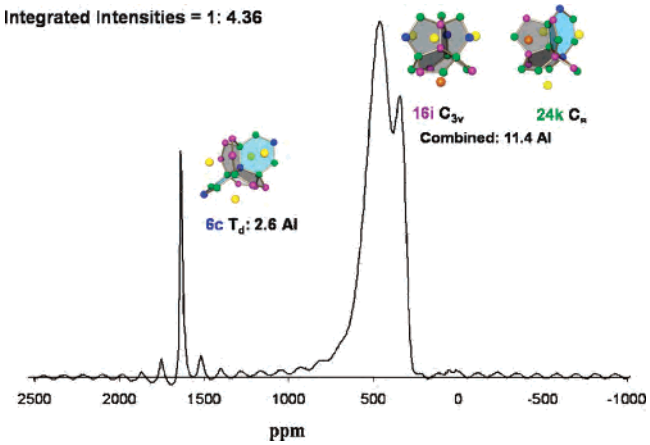

Figure 2. ^{27}Al MAS NMR for $Ba_8Al_{14}Si_{31}$. Figures represent the local site symmetry of the framework sites. The 6c sites are blue; the 16i sites are purple, and the 24k sites are green. The 2a sites are orange, and the 6d sites are yellow.

Figure 2 displays the ^{27}Al MAS NMR of $Ba_8Al_{14}Si_{31}$. All framework sites are represented in the spectrum. The peak at approximately 1600 ppm is symmetric and narrow, and the peak at 500 ppm exhibits a large quadrupolar pattern. Both signals are Knight shifted into the region of metallic aluminum indicating that Al in the framework is interacting with the conduction electrons. The peaks can be assigned on the basis of the local symmetry of the framework sites. The 6c site is highly symmetric and therefore would experience no electric-field gradient and no quadrupolar broadening. For these reasons, the narrow peak can be assigned to the 6c site. Sites responsible for the quadrupolar signal would experience a large asymmetric electric-field gradient. The framework site with the lowest local symmetry and highest degree of distortion is the 24k site. Therefore the 24k site is assigned to the quadrupole peak. Since the quadrupolar peak is broad, it is likely that the 16i site is also represented by this peak. This interpretation is similar to that reported for ^{71}Ga MAS NMR of $Ba_8Ga_{16}Ge_{30}$.[35] The integrated ratio of the signals is 1:4.36. If this corresponds to the total number of Al in the sample, then there are 2.6 Al at the 6c site and 11.4 Al in the combined 24k and 16i sites. From the occupancies in Table 3, obtained from the neutron diffraction analysis, the corresponding number of Al atoms on each site is 3.3, 4.3, and 6.5 for the 6c, 16i, and 24k sites, respectively. While the values for the Al site

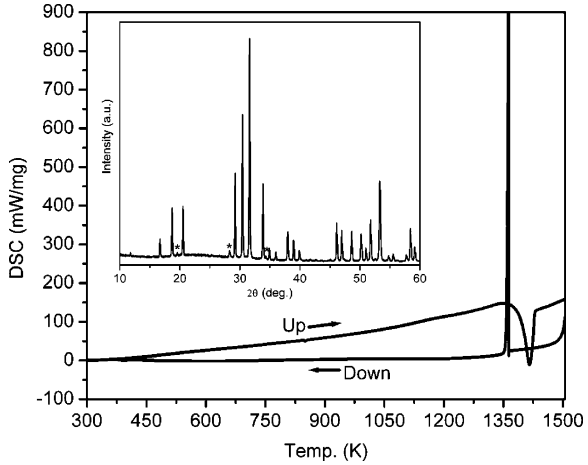

Figure 3. DSC (mV/mg) traces as a function of temperature for $Ba_8Al_{14}Si_{31}$. Data were obtained by heating at a rate of 4K/min under argon. The inset displays the powder X-ray diffraction pattern of $Ba_8Al_{14}Si_{31}$ after DSC measurement. * indicates a slight oxidation of sample at high temperatures.

occupancies are different between the two sets of data, the NMR results provide additional support for the preferential occupancy of the 6c site, along with the smaller amounts of Al on the 16i and 24k sites.

As mentioned previously, several phases with the stoichiometry, $Ba_8Al_xSi_{42-3/4x}[]_{4-1/4x}$ ($x = 8$, 12, 16) have been prepared via arc melting with $x = 12$ and 16 being incongruently melting phases. The lattice parameters increase as the amount of Al increases (from $x = 8$ to 16). The lattice parameters for our phase ($x = 14$) are nearly the same as those reported for $x = 16$. To further characterize this phase ($x = 14$), we also measured the melting behavior via TGA/DSC. The DSC scan for $Ba_8Al_{14}Si_{30}$ is displayed in Figure 3. The DSC trace suggests that this phase melts (endotherm) at 1416 K and recrystallizes at 1363 K (exotherm). There is no evidence for additional phase changes, so this clathrate phase melts congruently. Furthermore, there was no evidence of weight loss or weight gain in the TGA scans. X-ray powder diffraction of the sample after melting, inset of Figure 3, is consistent with this hypothesis. The fact that the sample melts congruently makes it ideal for large crystal growth and the high-temperature melting point makes it attractive for high-temperature applications.

The temperature dependence of the electrical resistivity and the Seebeck coefficient for $Ba_8Al_{14}Si_{31}$ are provided in Figure 4a and b, respectively. $Ba_8Al_{14}Si_{31}$ possesses n-type conductivity, and the electrical resistivity increases with increasing temperature characteristic of metallic behavior. This is similar to data reported for annealed pressed pellets of $Ba_8Al_xSi_{42-3/4x}[]_{4-1/4x}$ ($x = 8$, 12, 16), with $x = 16$ having a room temperature value of approximately 0.85 mΩ cm.[22] Our resistivity is lower, with a room-temperature value of 0.445 mΩ cm, as expected because no grain-boundary scattering should contribute in our single-crystal specimen. The absolute value of the Seebeck coefficient gradually increases with increasing temperature with a value of −21 μV/K at room temperature. The temperature dependence of the Seebeck coefficient for annealed pressed pellets of $Ba_8Al_{14}Si_{31}$ has been previously measured and gives a room-temperature value of ~ -49 μV/K.[21,22] This absolute value

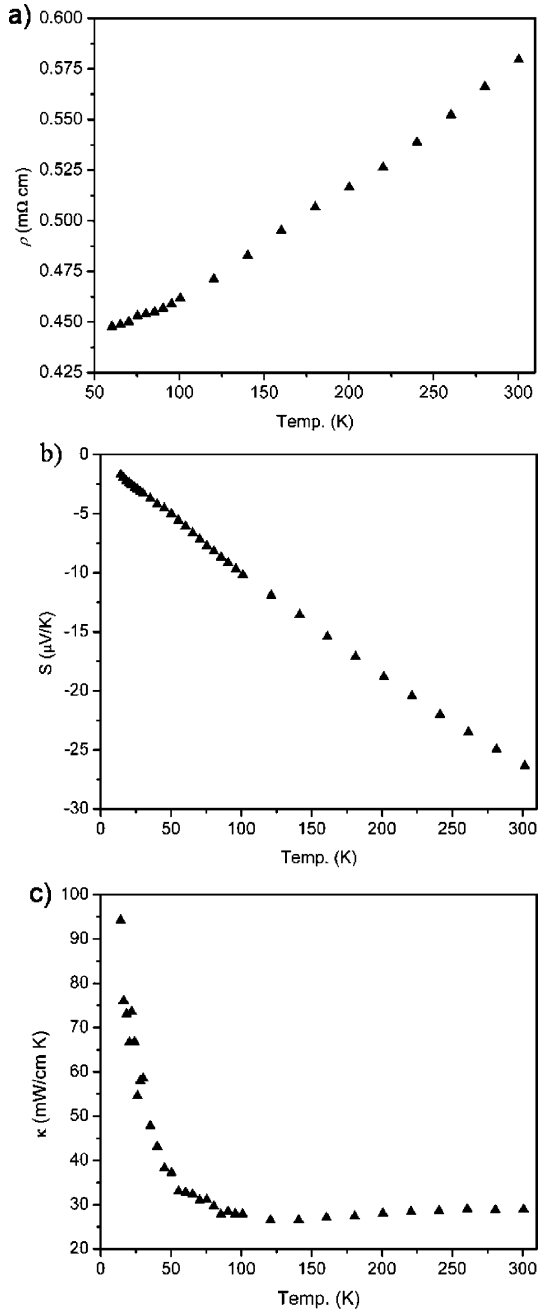

Figure 4. Shows the temperature dependence of the (a) resistivity, (b) the Seebeck coefficient, and (c) the thermal conductivity for $Ba_8Al_{14}Si_{31}$.

is higher than our measured room-temperature Seebeck coefficient and may indicate that the polycrystalline specimens are closer to the ideal stoichiometry of $Ba_8Al_{16}Si_{30}$.

Figure 4c shows the total thermal conductivity for $Ba_8Al_{14}Si_{31}$. $Ba_8Al_{14}Si_{31}$ exhibits low thermal conductivity, with values typical of clathrate phases but larger than the Ga−Ge phases, likely because of the smaller less-massive framework atoms forming smaller, lighter polyhedra. In addition, the temperature dependence of the data is similar to a crystalline rather than a glass phase. These data, taken together at 300 K, yield a zT for $Ba_8Al_{14}Si_{31}$ of 0.010 which is fairly low but not unexpected for a metallic clathrate phase. Adjustment of the carrier concentration via adjustment of the framework stoichiometry should improve the correspond-

ing electrical properties and may lead to improved *zT* values.[16,20,36,37] It may also be possible to improve these values by doping smaller atoms into the guest sites, diminishing guest−host interactions and therefore increasing the resonant scattering of phonons and thus lowering thermal conductivity.[12,14,16,17,38−41] Thus, *zT* values should be greatly improved upon optimization of these silicon clathrates.

Acknowledgment. The authors gratefully acknowledge Dr. Alexandra Navrotsky (Department of Chemistryand Thermochemistry Facility and NEAT ORU, University of California Davis) for use of the Scintag powder diffractometer, Dr. Ping Yu (Department of Materials Engineering, University of California Davis) for help with ^{27}Al MAS NMR, and H. Rubin (University of South Florida) for help with thermal conductivity. This research was funded by the NSF. Work at Argonne was supported by the U.S. Department of Energy, Basic Energy Sciences, Materials Sciences, under Contract W-31-109-Eng-38. C.L.C. acknowledges funding from a Tyco Electronics Foundation Fellowship for functional materials. G.S.N. and J.M. acknowledge support by the Department of Energy under Grant number DE-FG02-04ER46145 for transport measurements and analysis.

(36) Madsen, G. K. H.; Schwartz, K.; Blaha, P.; Singh, J. *Phys. Rev. B* **2003**, *68*, 125212.
(37) Bryan, J. D.; Blake, N. P.; Metiu, H.; Stucky, G. D.; Iversen, B. B.; Poulsen, R. D.; Bentien, A. *J. Appl. Phys.* **2002**, *92*, 7281.
(38) Sales, B. C.; Chakoumakos, B. C.; Jin, R.; Thompson, J. R.; Mandrus, D. *Phys. Rev. B* **2001**, *63*, 245113/245111.
(39) Blake, N. P.; Bryan, D.; Latturner, S.; Mollnitz, L.; Stucky, G. D.; Metiu, H. *J. Chem. Phys.* **2001**, *114*, 10063.
(40) Blake, N. P.; Latturner, S.; Bryan, J. D.; Stucky, G. D.; Metiu, H. *J. Chem. Phys.* **2002**, *116*, 9545.
(41) Blake, N. P.; Mollnitz, L.; Stucky, G. D.; Metiu, H. *Int. Conf. Thermoelectr.* **1999**, *18*, 489.
(42) Ozawa, T. C.; Kang, S. J. *J. Appl. Crystallogr.* **2004**, *37*, 679.

Supporting Information Available: Neutron crystallographic data in CIF format. This material is available free of charge via the Internet at http://pubs.acs.org.

IC061241W